



Effect of substrate geometry on liquid-crystal-mediated nanocylinder-substrate interactions

Title	Effect of substrate geometry on liquid-crystal-mediated nanocylinder-substrate interactions
Author(s)	Cheung, David L.;Allen, Michael P.
Publication Date	2008
Publisher	American Institute of Physics
Repository DOI	10.1063/1.2977968

Effect of substrate geometry on liquid-crystal-mediated nanocylinder-substrate interactions

David L. Cheung*

*Department of Chemistry and Centre for Scientific Computing,
University of Warwick, Coventry, CV4 7AL, UK*

Michael P. Allen†

*Department of Physics and Centre for Scientific Computing,
University of Warwick, Coventry, CV4 7AL, UK*

Abstract

Using classical density functional theory (DFT) the liquid crystal (LC)-mediated interaction between a cylindrical nanoparticle and a structured substrate is studied. The surface is structured by cutting a rectangular groove into the surface. In the absence of the nanoparticle, a range of defect structures are formed in the vicinity of the groove. By varying the groove width and depth the LC-mediated interaction changes from repulsive to attractive. This interaction is strongest when the groove is of comparable size to the nanoparticle. For narrow grooves the nanoparticle is attracted to the centre of the groove, while for wider grooves there is a free energy minimum near the side walls.

PACS numbers: 61.20.Gy,61.30.Cz,61.30.Jf

I. INTRODUCTION

The behaviour of dispersions of nm-scale particles (nanoparticles) in both simple and complex fluids is important in many areas of science and technology¹. The reduced dimensions of such particles result in properties that dramatically diverge from those of bulk materials. Advances in the synthesis of such nanometre sized particles have opened up a range of possibilities in materials science. One key issue is the formation of ordered structures from these nanoparticles². For colloidal particles, crystallization may be induced at solid substrates, with a range of crystal structures being observed. More complex structures may be formed at suitably templated surfaces³. For nanoparticles, similar techniques may be applied. However, due to their small size these are greatly complicated due to solvent effects.

Nanoparticles dispersed in nematic liquid crystals (LCs) are of much interest. The director field around a solid particle immersed in a nematic becomes distorted, with a range of defect structures, depending on particle size and shape, and anchoring conditions at the particle surface. These topological defects give rise to long-range interactions between immersed nanoparticles, which leads to a range of structures, including chains^{4,5}, clusters⁶, and periodic arrays⁷. As well as leading to the formation of such ordered structures, the fluidity of LCs allows the manipulation of immersed particles under external fields or bounding surfaces. This is being exploited in order to construct ordered arrays of nanoparticles and related particles such as carbon nanotubes⁸⁻¹⁰. Dispersions of nm-scale particles, such as synthetic nanoparticles^{11,12}, carbon nanotubes¹³, and clay platelets¹⁴ are being investigated for use in optoelectronic devices. Carbon nanotubes in discotic LC have also been investigated for applications in organic electronics¹⁵ and carbon-nanotube-lyotropic LC suspensions have been investigated, both as a means of nanotube alignment and also for applications in biotechnology¹⁶.

In addition to many experimental studies¹⁷, nanoparticles in LCs have been the subject of a number of theoretical studies using a variety of approaches. Molecular simulation has been used to study LC structure around single nanoparticles¹⁸⁻²¹ and interactions between small numbers of them²²⁻²⁴, but for larger systems becomes prohibitively expensive. Phenomenological Landau-de Gennes (LdG) theory has been used to study a range of LC-nanoparticle systems²⁵⁻³¹. However it is incapable of accounting for spatial variation in the

LC density, which for nanoparticles of comparable size to LC molecules may be of considerable importance. Classical Density Functional Theory (DFT) incorporates density variation and is computationally less expensive than simulations, and has been recently applied to LC-nanoparticles dispersions^{32–34} by us. Closely related to DFT is Integral Equation Theory (IET), which has also been recently applied to spherical nanoparticles in LCs^{35–37}, studying the colloid induced structure and interactions between them. However, IET does not produce spontaneously ordered phases, so these calculations were performed using (arbitrarily) weak aligning fields.

In many instances interactions between nanoparticles and solid substrates in LCs is important. As well as being used to form ordered nanoparticle arrays, this is of interest in LC biosensors^{38,39}. Recent work, using either LdG^{27,40,41} or DFT³³ have shown a repulsive LC-mediated interaction between a nanocylinder and a planar substrate. This arises due to an increase in elastic energy due to director deformations and excluded volume effects. LdG theory has also been applied to nanoparticles near substrates with cavities^{31,40}. For a range of cavity sizes the LC-mediated interaction changes from repulsive to attractive with the strength of this interaction varying with cavity size, with the strongest attraction found when the cavity size was comparable to the size of the nanoparticle. The interaction strength was also found to be dependent on the cavity shape³¹. However the neglect of density variation means that the particle sizes studied are significantly larger than the molecular dimensions. By using DFT we are able to study nm-sized particles, in regimes that are difficult to access experimentally.

II. THEORY

The DFT methodology used in this paper is fully outlined in previous work^{32–34} and will only be briefly described here. The liquid crystal solvent is modelled as a fluid of hard ellipsoids of aspect ratio $e = a/b = 15$ (in the rest of this paper $b = 1$ will be taken to be the unit of length). The grand potential of such a system may be written as⁴²

$$\begin{aligned} \beta\Omega[\rho(\mathbf{r}, \mathbf{u})] = & \int d\mathbf{r}d\mathbf{u} \rho(\mathbf{r}, \mathbf{u}) \{\log \rho(\mathbf{r}, \mathbf{u}) - 1\} + \beta F_{\text{ex}}[\rho(\mathbf{r}, \mathbf{u})] \\ & + \beta \int d\mathbf{r}d\mathbf{u} (V_{\text{ext}}(\mathbf{r}, \mathbf{u}) - \mu)\rho(\mathbf{r}, \mathbf{u}), \end{aligned} \quad (1)$$

where $\rho(\mathbf{r}, \mathbf{u})$ is the position- and orientation-dependent single particle density, $V_{\text{ext}}(\mathbf{r}, \mathbf{u})$ is the external potential, μ is the chemical potential, and $\beta = 1/k_B T$. The first term in eqn. (1) is the (exact) ideal free energy (FE). The second is the excess FE, which is generally unknown. Here we employ the Onsager approximation⁴³

$$\beta F_{\text{ex}}[\rho(\mathbf{r}, \mathbf{u})] = -\frac{1}{2} \int d\mathbf{r}_1 d\mathbf{r}_2 d\mathbf{u}_1 d\mathbf{u}_2 f(\mathbf{r}_{12}, \mathbf{u}_1, \mathbf{u}_2) \rho(\mathbf{r}_1, \mathbf{u}_1) \rho(\mathbf{r}_2, \mathbf{u}_2), \quad (2)$$

where $\mathbf{r}_{12} = \mathbf{r}_1 - \mathbf{r}_2$ and $f(\mathbf{r}_{12}, \mathbf{u}_1, \mathbf{u}_2) = \exp\{-\beta V(\mathbf{r}_{12}, \mathbf{u}_1, \mathbf{u}_2)\} - 1$ is the Mayer function. $V(\mathbf{r}_{12}, \mathbf{u}_1, \mathbf{u}_2)$ is the intermolecular potential, where $V = \infty$ ($f = -1$) when two molecules overlap and $V = 0$ ($f = 0$) otherwise. Although eqn. (2) is only exact for infinite elongations, previous studies⁴⁴ have shown that there is good agreement between Onsager theory and simulation for the elongation used in this study ($e = 15$). While this aspect ratio is larger than those of common LC molecules (which have typically $e \approx 4 - 8$), the behaviour of such molecules is expected to be qualitatively similar. More sophisticated DFTs⁴⁵⁻⁴⁷ are necessary to study these aspect ratios. As the intermolecular potential is purely repulsive, the phase behaviour is solely determined by the chemical potential. In this work $\beta\mu = 1.4$, well inside the nematic phase ($\beta\mu \approx 1.32$ for the model and parameters used in this work).

The external potential, representing a single cylindrical nanoparticle of radius R_c oriented along the y axis, is given by

$$V_{\text{ext}}(\mathbf{r}, \mathbf{u}) = V_{\text{ext}}(\mathbf{s}, \mathbf{u}) = \begin{cases} V_0 [\tanh(b/w)] & s - R_c < -b \\ \frac{1}{2} V_0 \left[\tanh\left(\frac{R_c - s}{w}\right) + \tanh(b/w) \right] & |s - R_c| < b \\ 0 & s - R_c > b \end{cases} \quad (3)$$

where $\mathbf{s} = (x, z)$, $s = |\mathbf{s}|$, $V_0 = 50k_B T$, and $w = b/5$. This represents a sharply varying repulsive potential acting on the ellipsoid centres of mass; it excludes the molecules from the cylinder and gives rise to homeotropic (normal) anchoring at the surface. The nanoparticle radius was $R_c = 15b$ (one molecular length). The relative sizes of the solvent molecules and nanoparticle are similar to those of typical LC ($a \approx 1.8$ nm) and typical inorganic nanoparticles¹⁷ or proteins⁴⁸ (3-20 nm). The substrate is similarly represented by a step function acting on the centres of the solvent molecules, which likewise gives rise to homeotropic alignment at the surface. Structure is introduced into the substrate by cutting a rectangular groove, with width w and depth d , as shown in Fig. 1.

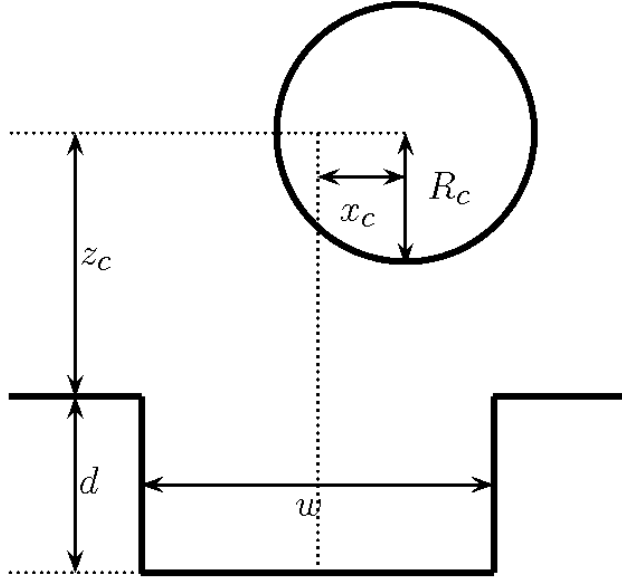


FIG. 1: Geometry of calculation

Following previous work³²⁻³⁴ the angularly dependent functions are expanded in a set of spherical harmonics, e.g. $\rho(\mathbf{r}, \mathbf{u}) = \sum_{\ell, m} \rho_{\ell m}(\mathbf{r}) Y_{\ell m}^*(\mathbf{u})$, $\log \rho(\mathbf{r}, \mathbf{u}) = \sum_{\ell, m} \tilde{\rho}_{\ell m}(\mathbf{r}) Y_{\ell m}(\mathbf{u})$, etc (note the complex conjugate in the density expansion). Similarly the Mayer function is expanded in rotational invariants. Inserting these expressions into eqn (1) and integrating over angles and the y direction gives the grand potential (per unit length along the y direction denoted as L)

$$\begin{aligned} \frac{\beta\Omega[\rho(\mathbf{r}, \mathbf{u})]}{L} &= \int d\mathbf{s} \sum_{\ell, m} \rho_{\ell m}(\mathbf{s}) \left(\tilde{\rho}_{\ell m}(\mathbf{s}) - \sqrt{4\pi}(1 + \beta\mu)\delta_{l0} + \beta V_{\ell m}(\mathbf{s}) \right) \\ &+ \int d\mathbf{s}_1 d\mathbf{s}_2 \sum_{\substack{\ell_1, m_1 \\ \ell_2, m_2}} \mathcal{L}_{\ell_1 m_1 \ell_2 m_2}(\mathbf{s}_{12}) \rho_{\ell_1 m_1}(\mathbf{s}_1) \rho_{\ell_2 m_2}(\mathbf{s}_2). \end{aligned} \quad (4)$$

The quantities $\mathcal{L}_{\ell_1 m_1 \ell_2 m_2}(\mathbf{s}_{12})$ come from integrating the Mayer function and are the spherical harmonic coefficients of the excluded length (in the y direction) of two molecules with a separation vector $\mathbf{s}_{12} = \mathbf{s}_1 - \mathbf{s}_2$ in the xz -plane, treated as a function of the molecular orientations. As the last term in eqn (4) is a convolution, it is most conveniently evaluated in reciprocal space. If $\rho_{\ell m}(\mathbf{k})$ is the two-dimensional Fourier transform of $\rho_{\ell m}(\mathbf{s})$ then this

term may be written

$$\sum_{\mathbf{k}} \sum_{\substack{\ell_1, m_1 \\ \ell_2, m_2}} \mathcal{L}_{\ell_1 m_1 \ell_2 m_2}(\mathbf{k}) \rho_{\ell_1 m_1}(\mathbf{k}) \rho_{\ell_2 m_2}(\mathbf{k}) \quad (5)$$

where $\mathcal{L}_{\ell_1 m_1 \ell_2 m_2}(\mathbf{k})$ is the Fourier transform of $\mathcal{L}_{\ell_1 m_1 \ell_2 m_2}(\mathbf{s}_{12})$.

In order to find the equilibrium density, the functions are tabulated on a regular grid in the xz plane; the grid spacing is $\delta x = \delta z = 0.5b$, the molecular length corresponding to 30 grid points. The grand potential is then minimised with respect to the $\tilde{\rho}_{\ell m}(\mathbf{s})$ coefficients at each grid point using the conjugate gradient method⁴⁹. When required, the coefficients $\rho_{\ell m}(\mathbf{s})$ are calculated from the spherical harmonics expansions, with angular integrations performed using Lebedev quadrature^{50,51}.

Once the equilibrium density coefficients $\rho_{\ell m}(\mathbf{s})$ have been determined, the number density $\rho(\mathbf{s})$ and order tensor $Q_{\alpha\beta}(\mathbf{s})$ may be found from

$$\rho(\mathbf{s}) = \int d\mathbf{u} \rho(\mathbf{s}, \mathbf{u}) = \sqrt{4\pi} \rho_{00}(\mathbf{s}) \quad (6)$$

$$Q_{\alpha\beta}(\mathbf{s}) = \frac{3}{2} \int d\mathbf{u} \rho(\mathbf{s}, \mathbf{u}) u_\alpha(\mathbf{s}) u_\beta(\mathbf{s}) - \frac{1}{2} \delta_{\alpha\beta}, \quad \alpha, \beta = x, y, z. \quad (7)$$

The spatially varying order parameter $S(\mathbf{s})$ is given by the largest eigenvalue of $Q_{\alpha\beta}(\mathbf{s})$ and the director $\mathbf{n}(\mathbf{s})$ by the eigenvector associated with $S(\mathbf{s})$. The LC mediated force (per unit length) on the nanoparticle may be found by differentiating the grand potential with respect to the nanoparticle coordinates^{52,53}. Explicitly the the force is given by³⁴

$$\frac{\beta \mathbf{F}}{L} = \int d\mathbf{s} \sqrt{4\pi} w^{-1} \operatorname{sech}^{-2} \left(\frac{R_c - |\mathbf{s} - \mathbf{S}_c|}{w} \right) \rho_{00}(\mathbf{s}) (\mathbf{s} - \mathbf{S}_c) \quad (8)$$

where the integration is over the region $|\mathbf{s} - \mathbf{S}_c| < R_c - b$.

III. RESULTS

A. Liquid crystals adsorbed at structured substrate

Shown in Fig. 2 are density and order parameter maps for nematic solvent in the absence of the cylinder. For shallow grooves (Fig. 2(a)) the director remains largely uniform in the vicinity of the surface. On increasing groove depth two small defects appear, due to competition between ordering at the groove sides and bottom. For the deepest, narrowest groove ($d = 30b$, $w = 30$) the LC inside the groove is aligned along the x -axis, due to

homeotropic alignment at the groove sides (Fig. 2(c)). This leads to a complex structure, with a large defect at the mouth of the groove and a second extended defect at the bottom of the groove. When the groove width is increased, this defect structure disappears, being replaced by two small defects near the groove sides. The defect structures for the $d = 15b$, $w = 30b$ and $d = 30b$, $w = 60b$ walls are similar to those found using LdG theory for grooves of the same aspect ratio³¹.

B. Variation of free energy with nanoparticle-substrate separation

The variation of Ω with z_c for different cell depths (for fixed width $w = 30b$) is shown in Fig. 3. For the flat planar substrate the interaction is short-ranged and largely repulsive³³, due to a combination of elastic and excluded volume interactions. The potential barrier and minimum near the surface arises due to overlap between the high density regions at the surface and around the nanoparticle. Similar behaviour is seen in simulation²⁷, but it is in contrast to predictions of LdG theory^{27,40}, due to the neglect of spatial density variation. $\Omega(z_c)$ for the $d = 5b$ wall shows similar behaviour. On increasing groove depth the nanocylinder-substrate interaction becomes attractive and increases in range. For groove depths up to $d = 15b$ the potential minimum, which is typically $2 - 3b$ from the groove bottom increases with d . For deeper grooves the potential minimum remains near the mouth of the groove $z_c \approx 3b$ (roughly the same position as the $d = 15b$ groove). This minimum however, is much shallower than for smaller d . When the cylinder moves inside the groove $\Omega(z_c)$ increases with a barrier at $z_c \approx -7.5b$ and a shallow minimum at $z_c \approx -13b$.

The variation in $\Omega(z_c)$ with cylinder separation for different groove widths is shown in Fig. 4. On increasing w for the $d = 15b$ groove the potential well first deepens then becomes shallower, with the deepest minimum for $w = 35b$. As the groove widens a potential barrier develops at $z_c \approx 10b$. For the $d = 30b$ groove there is an abrupt change in $\beta\Omega(z_c)$ on increasing w from $30b$ to $31b$, with the potential minimum at $z_c \approx -13b$ becoming deeper than the minimum at the groove mouth. The position of this (now) secondary minimum moves to lower z_c . For this and wider grooves the global minimum is inside the groove. As for the $d = 15b$ groove the potential minimum is deepest for $w = 35b$, with the secondary minimum being absent for $35b \leq w \leq 45b$ grooves. Shown in Fig. 5 is the potential minimum and minimum z_c as a function of w . For both $d = 15b$ and $d = 30b$ the lowest free energy is

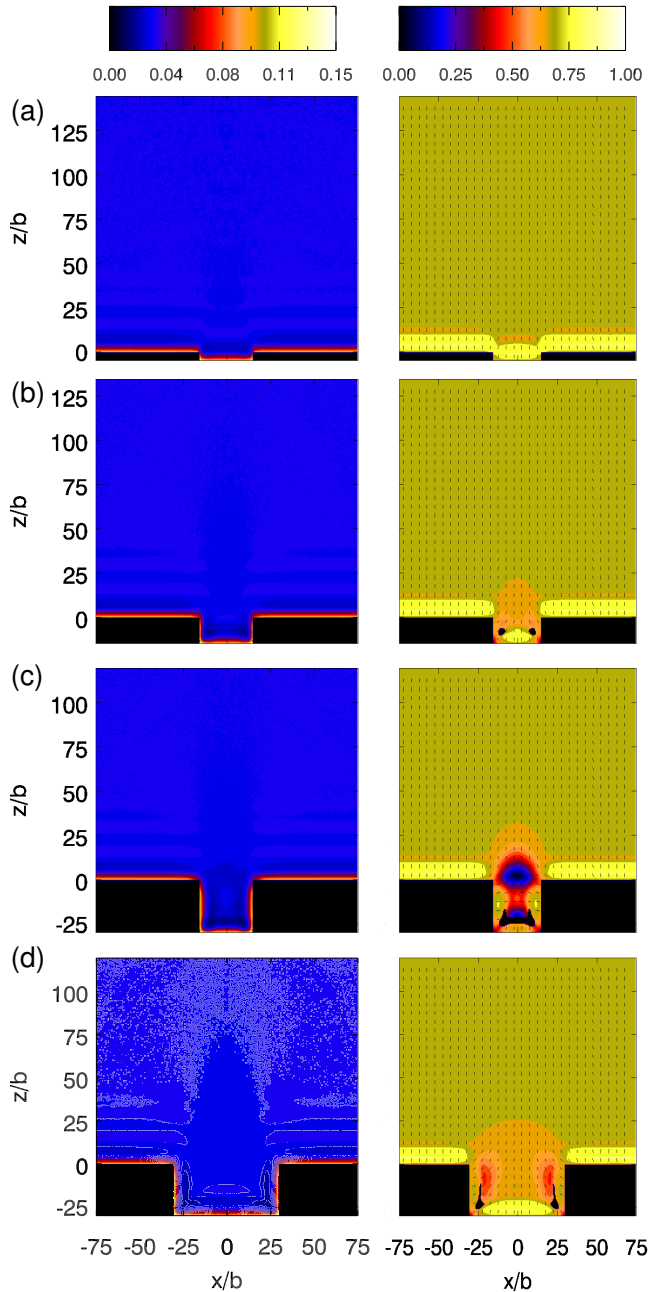


FIG. 2: (Colour online) Density (left) and order parameter (right) maps of LC solvent in contact with surface (in absence of cylinder), for groove dimensions (a) $d = 5b$, $w = 30b$, (b) $d = 15b$, $w = 30b$, (c) $d = 30b$, $w = 30b$, and (d) $d = 30b$, $w = 60b$.

found for the $w = 35b$ groove, with rapid variation in Ω_{min} around this. For a nanoparticle in the centre of a groove with large w the influence of the side walls becomes increasingly small and the interaction becomes that of a nanoparticle and flat substrate. This has been observed using LdG theory for spherical nanoparticles of spherical nanoparticles (radius 10

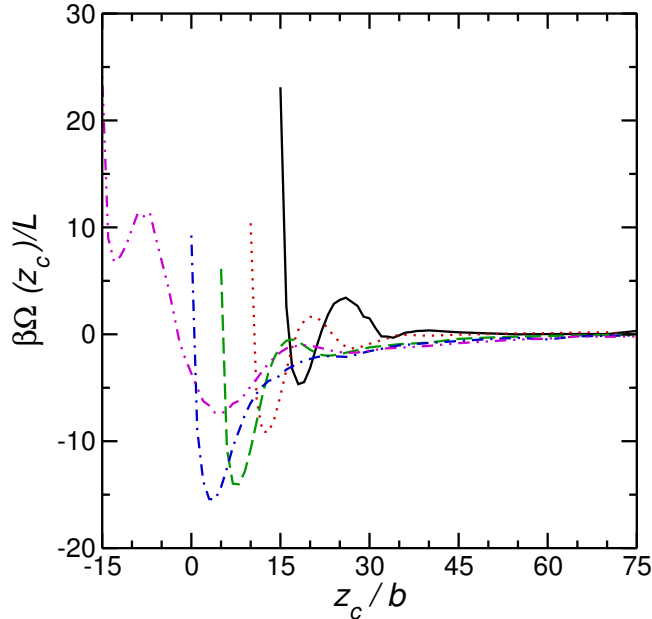


FIG. 3: (Colour online) Grand potential (per unit length) against separation (z_c) for wells of width $w = 30b$ and depths $d = 0b$ (solid line, black), $d = 5b$ (dotted line, red), $d = 10b$ (dashed line, green), $d = 15b$ (dot-dashed line, blue), and $d = 30b$ (double-dot-dashed line).

nm) in much larger channels³¹. With the exception of the narrowest groove, the free energy minimum position lies inside the groove for $d = 30b$.

The cylinder-substrate potential may be understood through changes in the LC-structure with cylinder separation. Shown in Fig. 6 are density and order parameters maps of the LC around cylinders in their potential minima. When the cylinder is located at the mouth of the $d = 30b$, $w = 30b$ groove ($z_c = 50b$) (Fig. 6a) the large defect found for the surface without cylinder (Fig. 2d) is absent. The radial anchoring at the surface of the cylinder causes the fluid in the groove to lie along the z direction. Two small defects appear near the sides of the groove due to the mismatch between homeotropic anchoring at the groove sides and the anchoring at the bottom of the groove. When the cylinder moves deeper into the groove ($z_c = 33b$) the structure is simpler, with two defects in the cusps between the cylinder and groove sides. When w is increased to $35b$ bridges of dense fluid appear between the cylinder and groove walls and the defects move away from the cylinder. These regions of high density and order lead to a decrease in the free energy. As w is increased further the bridges become more diffuse and have disappeared for $w = 60b$. The defects remain attached to the sharp corners of the groove³¹ and become larger.

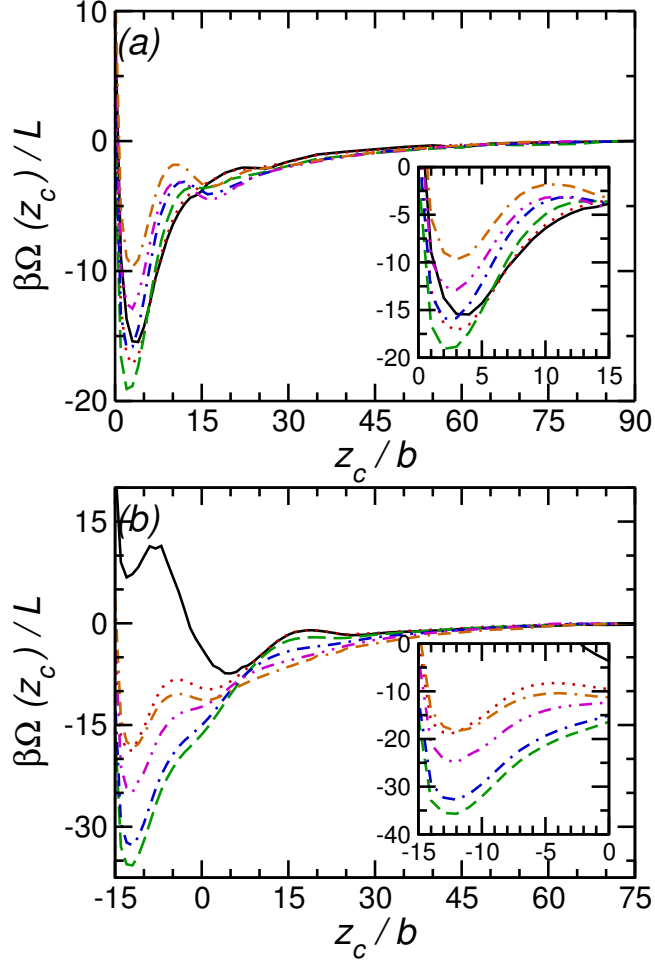


FIG. 4: (Colour online) Grand potential (per unit length) against z_c for wells of depth (a) $d = 15b$ and (b) $d = 30b$. In both cases $w = 30b$ is denoted by solid line (black), $w = 31b$ dotted line (red), $w = 35b$ dashed line (green), $w = 40b$ dot-dashed line (blue), $w = 45b$ double-dot-dashed line (magenta), and $w = 60b$ dot-double-dashed line (orange). Insets show details near free energy minima.

C. Variation of free energy within groove

In the previous calculations the cylinder was held equidistant from the groove walls. In Fig. 7 the variation in the grand potential as the cylinder is moved along the groove bottom ($z_c = 0$ for the $d = 15b$ and $z_c = -15b$ for the $d = 30b$ grooves). For narrow grooves ($d \leq 40b$) $\beta\Omega(x_c)$ has a minimum in the groove centre, while for wider grooves $\beta\Omega(x_c)$ has a maximum in the centre with minima near the groove walls. Such attraction into corners of wide wells has been observed experimentally in hard sphere colloids⁵⁴.

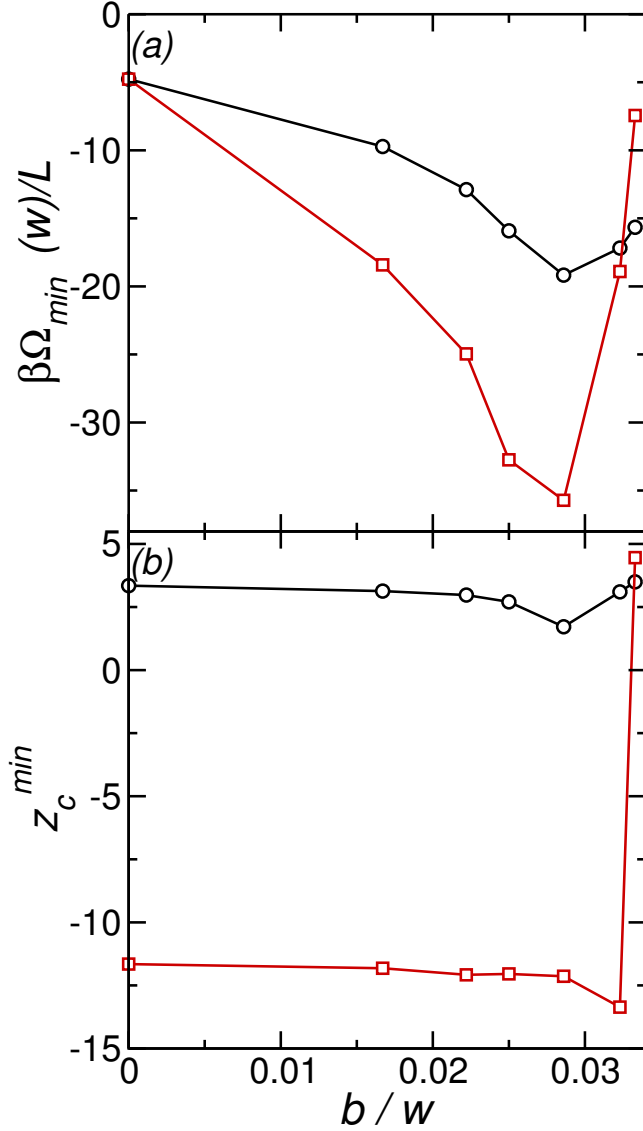


FIG. 5: (Colour online) Minimum grand potential (left) and minimum position (right) against $1/w$ for $d = 15b$ (circles, online black) and $d = 30b$ (squares, online red) grooves. The $1/w = 0$ point corresponds to a flat surface. The lines are a guide to the eye.

D. Variation of free energy with lateral displacement

The variation of Ω and force with lateral displacement, x_c , (for fixed $z_c = 15b$) is shown in Fig. 8. Figure 9 show the LC-structure around the nanoparticle and different grooves with $x_c \neq 0$. Far from the groove $\Omega(x_c)$ is constant. For wider grooves there is a free energy barrier on decreasing x_c (Fig. 8(a)). This is caused by the formation of a large defect near the groove side (Fig. 9(a)). A similar barrier was also seen in LdG theory calculations⁴⁰.

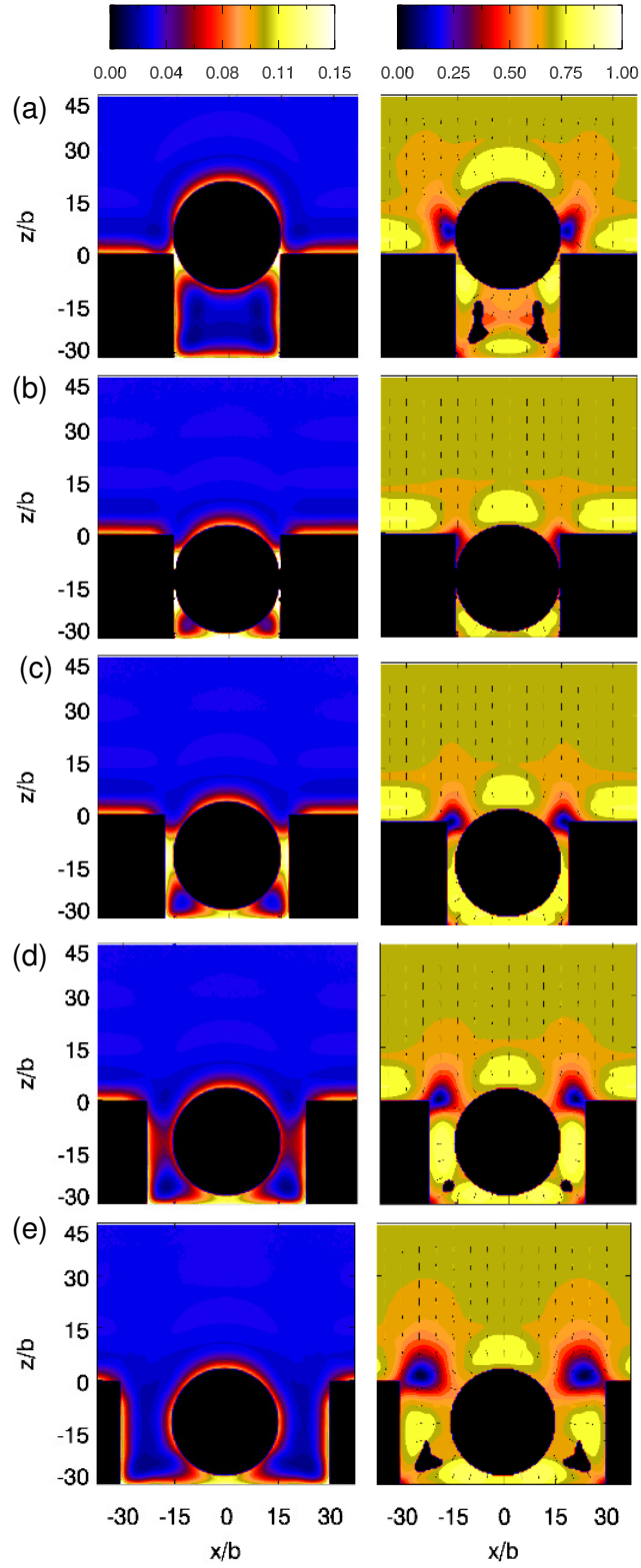


FIG. 6: (Colour online) Density (left) and order parameter (right) maps for (a) $d = 30b$, $w = 30b$, $z_c = 50b$, (b) $d = 30b$, $w = 30b$, $z_c = 32b$, (c) $d = 30b$, $w = 35b$, $z_c = 33b$, (d) $d = 30b$, $w = 45b$, $z_c = 33b$, and (e) $d = 30b$, $w = 60b$, $z_c = 33b$.

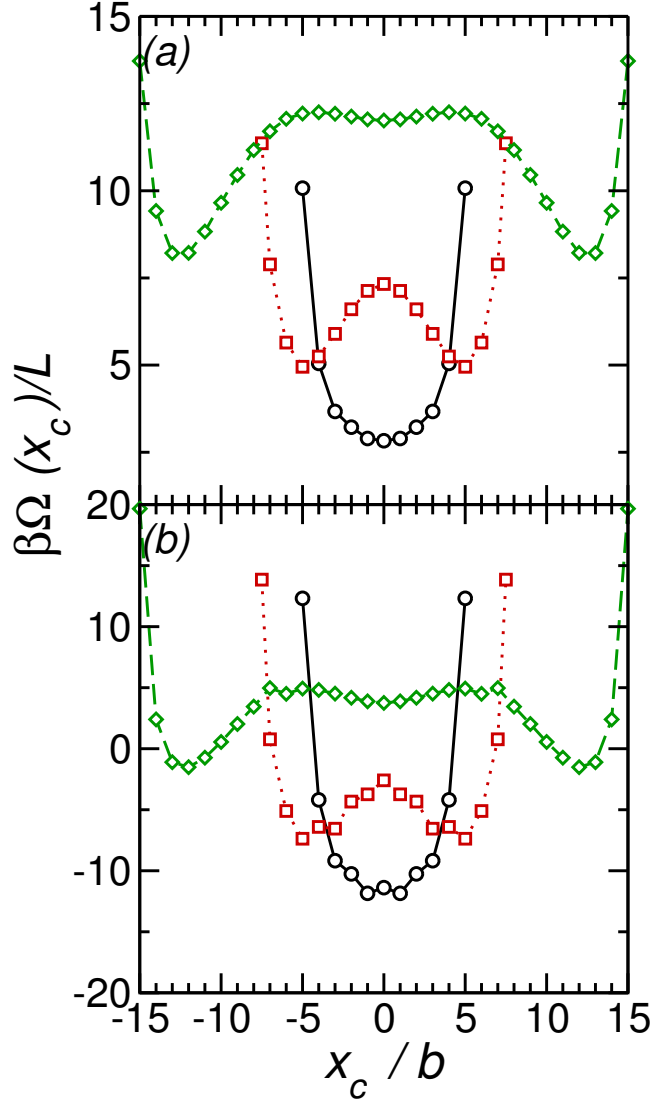


FIG. 7: (Colour online) Variation of grand potential for nanoparticle with $z_c = 0b$ for groove depth (a) $d = 15b$ and (b) $d = 30b$. For both graphs widths $w = 40b$ (circles, online black), $w = 45b$ (squares, online red), and $w = 60b$ (diamonds, online red).

In this region rapid variation in the lateral force is also seen (Fig. 8(b)). For narrower grooves this barrier is much smaller for $d = 15b$ and completely absent for $d = 30b$. The barrier disappears for this groove due the relief of the director frustration at the mouth of the groove (Fig. 9(c)).

On decreasing x_c $\Omega(x_c)$ drops rapidly. For $x_c \approx -22.5b$ ($w = 60b$) or $x_c \approx -7.5b$ ($w = 30b$) there is a potential minimum due to the formation of a high density bridge between the nanoparticle and groove corner (Fig. 9(b)). For the $w = 30b$ grooves this is the

minimum energy position ($\beta\Omega(x_c = -7.5b)/L - \beta\Omega(x_c = 0)/L \approx 1$). For the wider grooves this is a very shallow local minimum, with the energy being lowest when the nanoparticle is over the centre of the groove. The z -component of the force (Fig. 8(c)) is large and positive for large lateral displacements, due to the repulsion between a nanoparticle and a planar substrate. When the centre of the nanoparticle moves past the groove wall, F_z rapidly decreases, with there being a weak attraction towards the groove bottom.

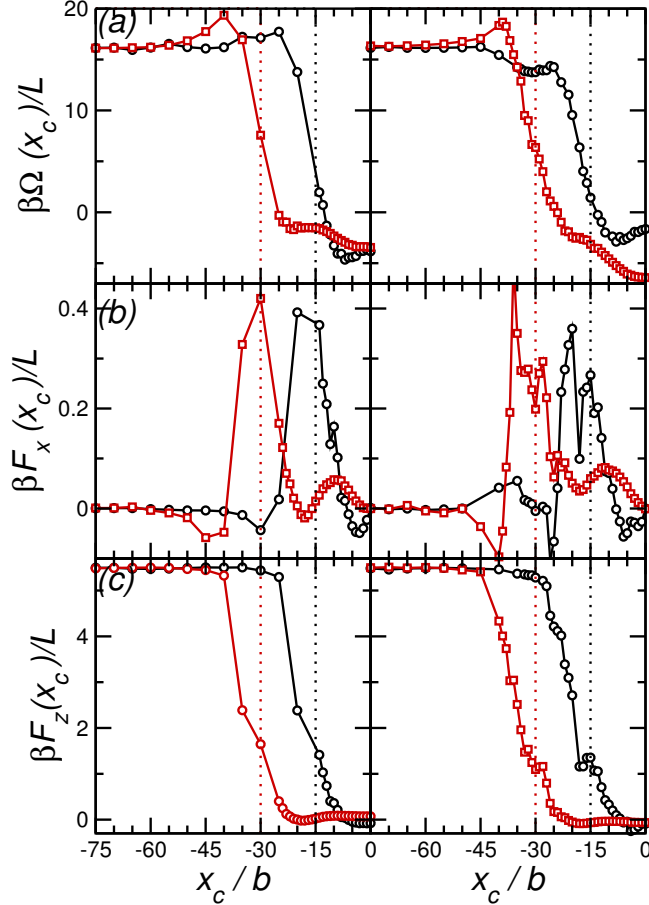


FIG. 8: (Colour online) (a) Variation of grand potential with lateral displacement for groove depth $d = 15b$ (left) and $d = 30b$ (right). In both cases width $w = 30b$ (circles, black) and $w = 60b$ (squares red). (b) x -component of force for groove depth $d = 15b$ (left) and $d = 30b$ (right). Symbols as in (a). (c) z -component of force for $d = 15b$ (left) and $d = 30b$ (right). Symbols as in (a). In all graphs the position of the groove edge is denoted by the dotted vertical lines (online $w = 30b$ groove red, $w = 60b$ groove green).

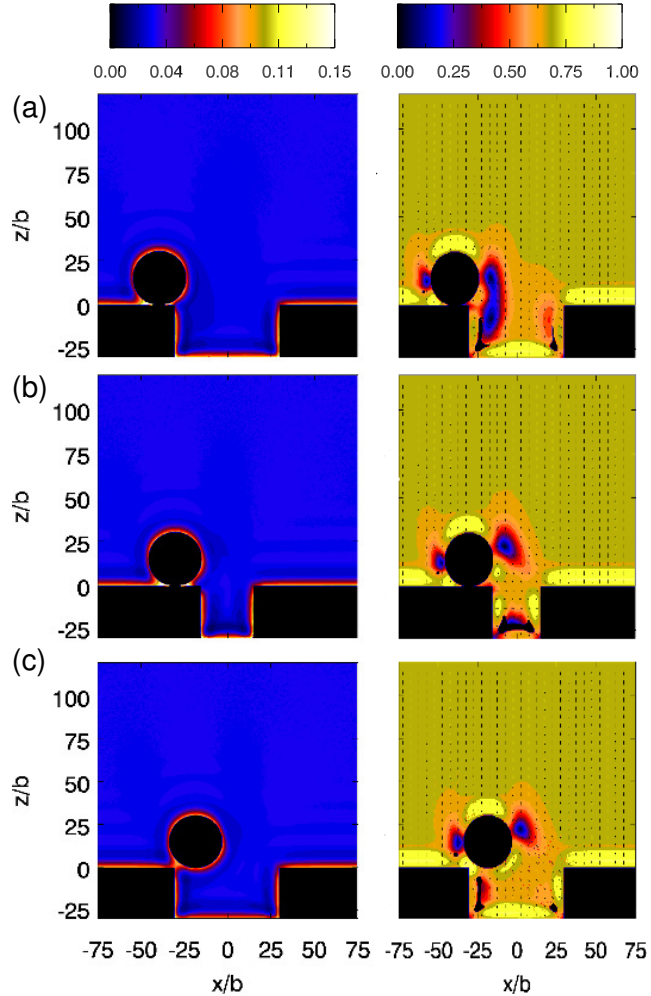


FIG. 9: (Colour online) (a) Density (left) and order parameter (right) maps for nanoparticle coordinates $x_c = -39b$, $z_c = 15b$ for groove dimensions $d = 30b$ and $w = 60b$. (b) Density (left) and order parameter (right) maps for nanoparticle coordinates $x_c = -30b$, $z_c = 15b$ for $d = 30b$, $w = 30b$ groove. (c) as (a) for $x_c = -18b$

IV. CONCLUSIONS

Using classical DFT the interaction between a cylindrical nanoparticle and a structured substrate has been studied. In the absence of a nanoparticle competition between anchoring at the groove sides and bottom sets up a complex defect structure for a range of groove widths and depths.

The nanoparticle-substrate interaction was found to be sensitive to changes in the substrate geometry. For a flat substrate the interaction is short-ranged and repulsive, due to

distortions in the LC director field³³. By cutting a rectangular groove in the substrate the interaction becomes attractive and longer ranged. This interaction is strongest for a groove width slightly larger than the nanoparticle diameter. The depth of the potential well varies rapidly with groove width around this minimal value. For narrow grooves the equilibrium position for the nanoparticle is in the groove centre, while for wider grooves the nanoparticle is attracted towards the groove walls. The variation with free energy with lateral displacement also depends on substrate geometry. For wider substrates a potential barrier appears on decreasing lateral displacement, due to formation of a defect near the groove corner. For narrower grooves this barrier is smaller and was absent for the $d = 30b$, $w = 30b$ grooves as the presence of the nanoparticle at the side of the groove relieves the director distortion at the mouth of the groove. $\Omega(x_c)$ drops rapidly due elimination of this defect and formation of a high density bridge between the groove corner and nanoparticle. For wider grooves this is a local minimum, with $\Omega(x_c)$ being lowest when $x_c = 0$, while for narrower grooves there is a weak potential maximum at $x_c = 0$.

The size-selectivity of the nanoparticle-substrate interaction is reminiscent of ‘key-lock’ mechanisms seen in biological systems. As the interaction strength varies rapidly with changes in groove geometry, such structured substrates may be used for sorting particles and for the nucleation of nanoparticle crystals. As well as depending on the groove geometry size, the interaction will also be dependent on nanoparticle size and shape, which has not been investigated in this work. It would also be interesting to investigate systems of several nanoparticles in and near grooved substrates³¹. Also of interest would be the behaviour near the nematic-isotropic transition, as studied for the planar wall in Ref.³⁴.

Acknowledgements

This research was supported by UK EPSRC (grants GR/S77240 and EP/E03375X) and the calculations were performed on the computing facilities of the Centre for Scientific Computing, University of Warwick.

* Electronic address: david.cheung@warwick.ac.uk

† Electronic address: m.p.allen@warwick.ac.uk

- ¹ G. A. Ozin and A. Arsenault, *Nanochemistry: A chemical approach to nanomaterials* (RSC, Cambridge, 2005).
- ² H. Zhang, E. W. Edwards, D. Y. Wang, and H. Möhwald, *Phys. Chem. Chem. Phys.* **8**, 3288 (2006).
- ³ D. Wang and H. Möhwald, *J. Mater. Chem.* **14**, 459 (2004).
- ⁴ P. Poulin, H. Stark, T. C. Lubensky, and D. A. Weitz, *Science* **275**, 1770 (1997).
- ⁵ J.-C. Loudet, P. Barios, and P. Poulin, *Nature* **407**, 611 (2000).
- ⁶ V. G. Nazarenko, A. B. Nych, and B. I. Lev, *Phys. Rev. Lett.* **87**, 077504/1 (2001).
- ⁷ I. Muševič, M. Skarabot, U. Tkalec, M. Ravnik, and S. Zumer, *Science* **313**, 954 (2006).
- ⁸ M. Lynch and D. Patrick, *Nano. Lett.* **2**, 1197 (2002).
- ⁹ I. Dierking, G. Scalia, and P. Morales, *J. Appl. Phys.* **97**, 044309/1 (2005).
- ¹⁰ I. Dierking, G. Scalia, P. Morales, and D. LeClare, *Adv. Mater.* **16**, 865 (2004).
- ¹¹ J. Müller, C. Sönnichsen, H. von Poschinger, G. von Plessen, T. A. Klar, and J. Feldmann, *Appl. Phys. Lett.* **81**, 171 (2002).
- ¹² S.-C. Jeng, C.-W. Kuo, H.-L. Wang, and C.-C. Liao, *Appl. Phys. Lett.* **91**, 061112/1 (2007).
- ¹³ I. Dierking and S. E. San, *Appl. Phys. Lett.* **87**, 233507/1 (2005).
- ¹⁴ J. S. van Duijneveldt, S. Klein, E. Leach, C. Pizzey, and R. M. Richardson, *J. Phys. Cond. Mat.* **17**, 2255 (2005).
- ¹⁵ S. Kumar and H. R. Bisoyi, *Angew. Chem.* **46**, 1501 (2007).
- ¹⁶ J. Lagerwall, G. Scalia, M. Haluska, U. Dettlaff-Weglikowska, S. Roth, and F. Giesselmann, *Adv. Mater.* **19**, 359 (2007).
- ¹⁷ T. Hegmann, H. Qi, and V. M. Marx, *J. Inorg. Organomet. Polym.* **17**, 483 (2007).
- ¹⁸ J. L. Billeter and R. A. Pelcovits, *Phys. Rev. E* **62**, 711 (2000).
- ¹⁹ D. Andrienko, G. Germano, and M. P. Allen, *Phys. Rev. E* **63**, 041701/1 (2001).
- ²⁰ D. Andrienko, M. P. Allen, G. Skačej, and S. Žumer, *Phys. Rev. E* **65**, 041702/1 (2002).
- ²¹ E. B. Kim, R. Faller, Q. Yan, N. L. Abbot, and J. J. de Pablo, *J. Chem. Phys.* **117**, 7781 (2002).
- ²² M. Al-Barwani, G. Sutcliffe, and M. Allen, *J. Phys. Chem. B* **108**, 6663 (2004).
- ²³ O. Guzmán, E. B. Kim, S. Grollau, N. L. Abbott, and J. J. de Pablo, *Phys. Rev. Lett.* **91**, 235507/1 (2003).
- ²⁴ E. B. Kim, O. Guzmán, S. Grollau, N. L. Abbott, and J. J. de Pablo, *J. Chem. Phys.* **121**, 1949 (2004).

- ²⁵ P. Patrício, M. Tasinkevych, and M. M. Telo da Gama, *Euro. Phys. J. E* **7**, 117 (2002).
- ²⁶ M. Tasinkevych, N. M. Silvestre, P. Patrício, and M. M. Telo da Gama, *Euro. Phys. J. E* **9**, 341 (2002).
- ²⁷ S. Grollau, E. B. Kim, O. Guzmán, N. L. Abbott, and J. J. de Pablo, *J. Chem. Phys.* **119**, 2444 (2003).
- ²⁸ D. Andrienko, M. Tasinkevych, P. Patricio, M. P. Allen, and M. M. Telo da Gama, *Phys. Rev. E* **68**, 051702/1 (2003).
- ²⁹ D. Andrienko, M. Tasinkevych, P. Patrício, and M. M. T. da Gama, *Phys. Rev. E* **69**, 021706/1 (2004).
- ³⁰ J.-i. Fukuda, H. Stark, M. Yoneya, and H. Yokoyama, *Phys. Rev. E* **69**, 041706 (2004).
- ³¹ F. R. Hung, B. T. Gettelfinger, J. Gary M. Koenig, N. L. Abbott, and J. J. de Pablo, *J. Chem. Phys.* **127**, 124702/1 (2007).
- ³² D. L. Cheung and M. P. Allen, *Phys. Rev. E* **74**, 021701/1 (2006).
- ³³ D. L. Cheung and M. P. Allen, *Phys. Rev. E* **76**, 041706/1 (2007).
- ³⁴ D. L. Cheung and M. P. Allen, *Langmuir* **24**, 1411 (2008).
- ³⁵ T. G. Sokolovska, R. O. Sokolovskii, and G. N. Patey, *J. Comp. Phys.* **122**, 124907 (2005).
- ³⁶ T. G. Sokolovska, R. O. Sokolovskii, and G. N. Patey, *Phys. Rev. E* **73**, 020701 (2006).
- ³⁷ T. G. Sokolovska, R. O. Sokolovskii, and G. N. Patey, *Phys. Rev. E* **77**, 041701 (2008).
- ³⁸ V. K. Gupta, J. J. Skaife, T. B. Dubrovsky, and N. L. Abbot, *Science* **279**, 2077 (1998).
- ³⁹ T. Govindaraju, P. J. Bertics, R. T. Raines, and N. L. Abbot, *J. Am. Chem. Soc.* **129**, 11223 (2007).
- ⁴⁰ N. M. Silvestre, P. Patricio, and M. M. T. da Gama, *Phys. Rev. E* **69**, 061402/1 (2004).
- ⁴¹ G. McKay and E. G. Virga, *Phys. Rev. E* **71**, 041702/1 (2005).
- ⁴² J.-P. Hansen and I. R. McDonald, *Theory of Simple Liquids* (Academic Press, London, 1986), 2nd ed.
- ⁴³ L. Onsager, *Ann. N. Y. Acad. Sci.* **51**, 627 (1949).
- ⁴⁴ P. J. Camp, C. P. Mason, M. P. Allen, A. A. Khare, and D. A. Kofke, *J. Chem. Phys.* **105**, 2837 (1996).
- ⁴⁵ A. M. Somoza and P. Tarazona, *J. Chem. Phys.* **91**, 517 (1989).
- ⁴⁶ G. Cinacchi and F. Schmid, *J. Phys. Cond. Mat.* **14**, 12223 (2002).
- ⁴⁷ A. Esztermann, H. Reich, and M. Schmidt, *Phys. Rev. E* **73**, 011409/1 (2006).

- ⁴⁸ J. J. Skaife, J. M. Brake, and N. L. Abbott, *Langmuir* **17**, 5448 (2001).
- ⁴⁹ W. H. Press, B. P. Flannery, S. A. Teukolsky, and W. T. Vetterling, *Numerical Recipes* (Cambridge University Press, Cambridge, 1986).
- ⁵⁰ V. I. Lebedev, *Zh. Vychisl. Mat. Mat. Fiz* **16**, 293 (1976), (English translation: *USSR Comput. Math. & Math. Phys.* 16, 10 (1976)).
- ⁵¹ V. I. Lebedev, *Sibirskii Matematicheskii Zhurnal* **18**, 132 (1977).
- ⁵² H. Löwen, P. A. Madden, and J.-P. Hansen, *Phys. Rev. Lett.* **68**, 1081 (1992).
- ⁵³ H. Löwen, J.-P. Hansen, and P. A. Madden, *J. Chem. Phys.* **98**, 3275 (1993).
- ⁵⁴ A. D. Dinsmore and A. G. Yodh, *Langmuir* **15**, 314 (1999).

Figure Captions

- Fig. 1. Geometry of calculation
- Fig. 2. (Colour online) Density (left) and order parameter (right) maps of LC solvent in contact with surface (in absence of cylinder), for groove dimensions (a) $d = 5b$, $w = 30b$, (b) $d = 15b$, $w = 30b$, (c) $d = 30b$, $w = 30b$, and (d) $d = 30b$, $w = 60b$.
- Fig. 3. (Colour online) Grand potential (per unit length) against separation (z_c) for wells of width $w = 30b$ and depths $d = 0b$ (solid line, black), $d = 5b$ (dotted line, red), $d = 10b$ (dashed line, green), $d = 15b$ (dot-dashed line, blue), and $d = 30b$ (double-dot-dashed line).
- Fig. 4. (Colour online) Grand potential (per unit length) against z_c for wells of depth (a) $d = 15b$ and (b) $d = 30b$. In both cases $w = 30b$ is denoted by solid line (black), $w = 31b$ dotted line (red), $w = 35b$ dashed line (green), $w = 40b$ dot-dashed line (blue), $w = 45b$ double-dot-dashed line (magenta), and $w = 60b$ dot-double-dashed line (orange). Insets show details near free energy minima.
- Fig. 5. (Colour online) Minimum grand potential (left) and minimum position (right) against $1/w$ for $d = 15b$ (circles, online black) and $d = 30b$ (squares, online red) grooves. The $1/w = 0$ point corresponds to a flat surface. The lines are a guide to the eye.
- Fig. 6. (Colour online) Density (left) and order parameter (right) maps for (a) $d = 30b$, $w = 30b$, $z_c = 50b$, (b) $d = 30b$, $w = 30b$, $z_c = 32b$, (c) $d = 30b$, $w = 35b$, $z_c = 33b$, (d) $d = 30b$, $w = 45b$, $z_c = 33b$, and (e) $d = 30b$, $w = 60b$, $z_c = 33b$.
- Fig. 7. (Colour online) Variation of grand potential for nanoparticle with $z_c = 0b$ for groove depth (a) $d = 15b$ and (b) $d = 30b$. For both graphs widths $w = 40b$ (circles, online black), $w = 45b$ (squares, online red), and $w = 60b$ (diamonds, online red).
- Fig. 8. (Colour online) (a) Variation of grand potential with lateral displacement for groove depth $d = 15b$ (left) and $d = 30b$ (right). In both cases width $w = 30b$ (circles, black) and $w = 60b$ (squares red). (b) x -component of force for groove depth $d = 15b$ (left) and $d = 30b$ (right). Symbols as in (a). (c) z -component of force for $d = 15b$ (left) and $d = 30b$ (right). Symbols as in (a). In all graphs the position of the groove edge

is denoted by the dotted vertical lines (online $w = 30b$ groove red, $w = 60b$ groove green).

Fig. 9. (Colour online) (a) Density (left) and order parameter (right) maps for nanoparticle coordinates $x_c = -39b$, $z_c = 15b$ for groove dimensions $d = 30b$ and $w = 60b$. (b) Density (left) and order parameter (right) maps for nanoparticle coordinates $x_c = -30b$, $z_c = 15b$ for $d = 30b$, $w = 30b$ groove. (c) as (a) for $x_c = -18b$

Fig. 1 D. L. Cheung and M. P. Allen

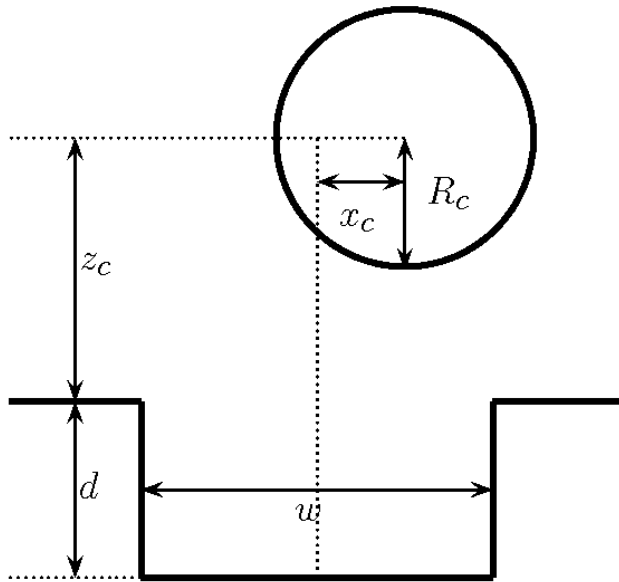


Fig. 2 D. L. Cheung and M. P. Allen

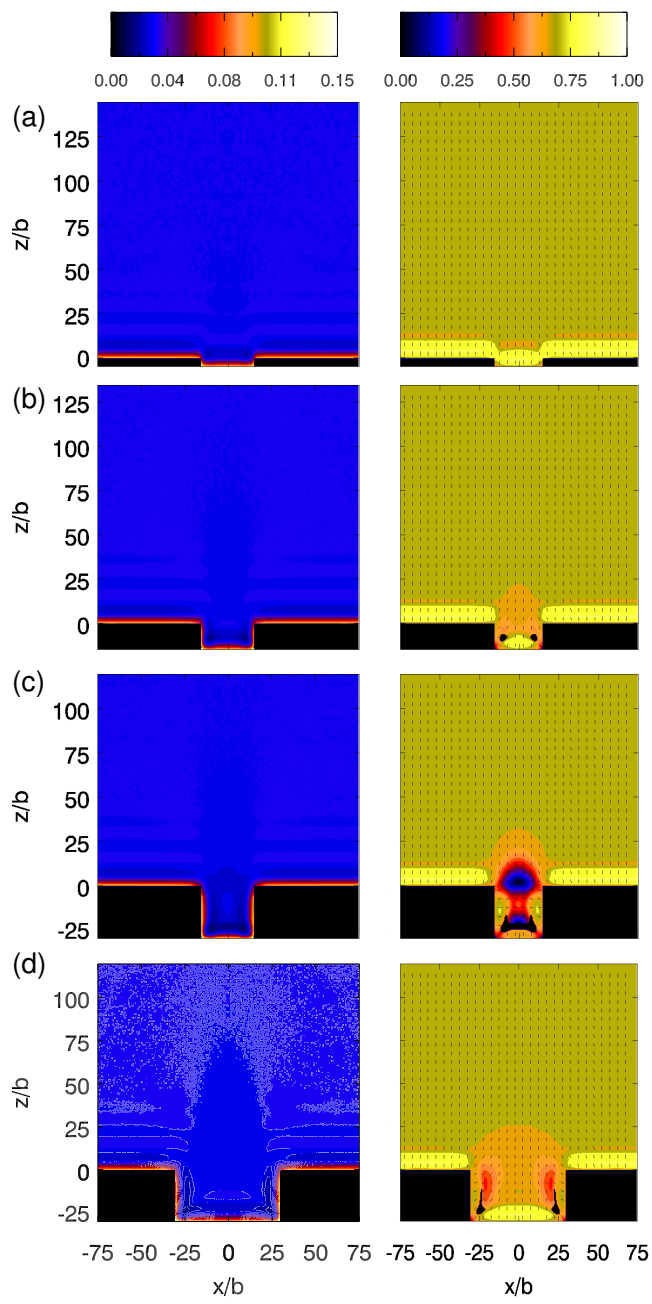


Fig. 3 D. L. Cheung and M. P. Allen

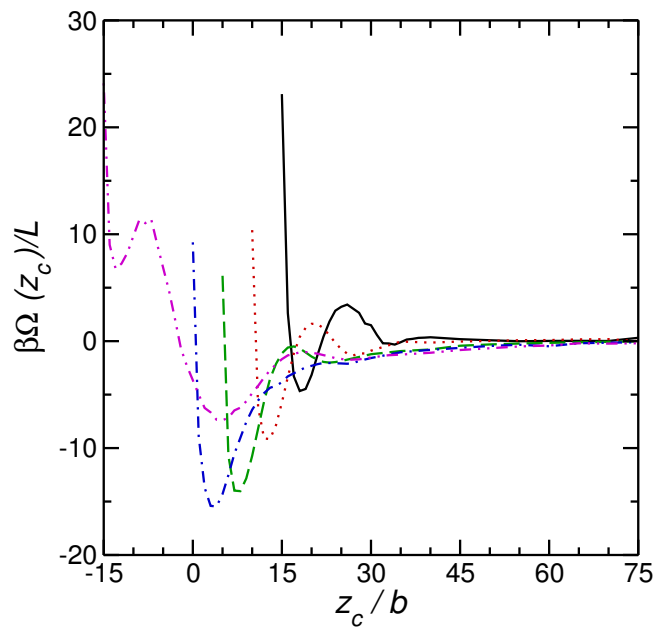


Fig. 4 D. L. Cheung and M. P. Allen

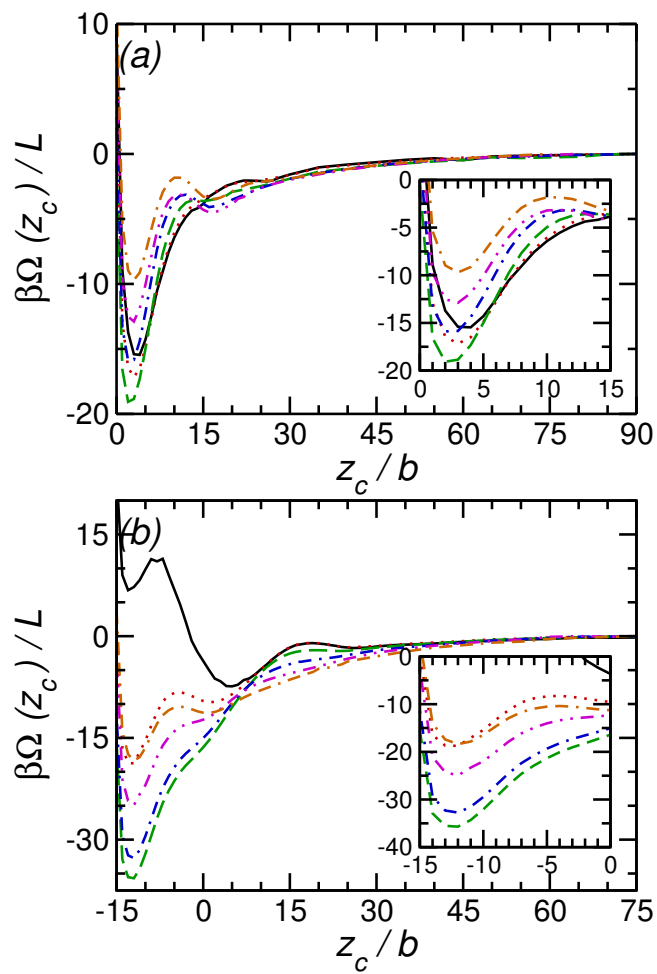


Fig. 5 D. L. Cheung and M. P. Allen

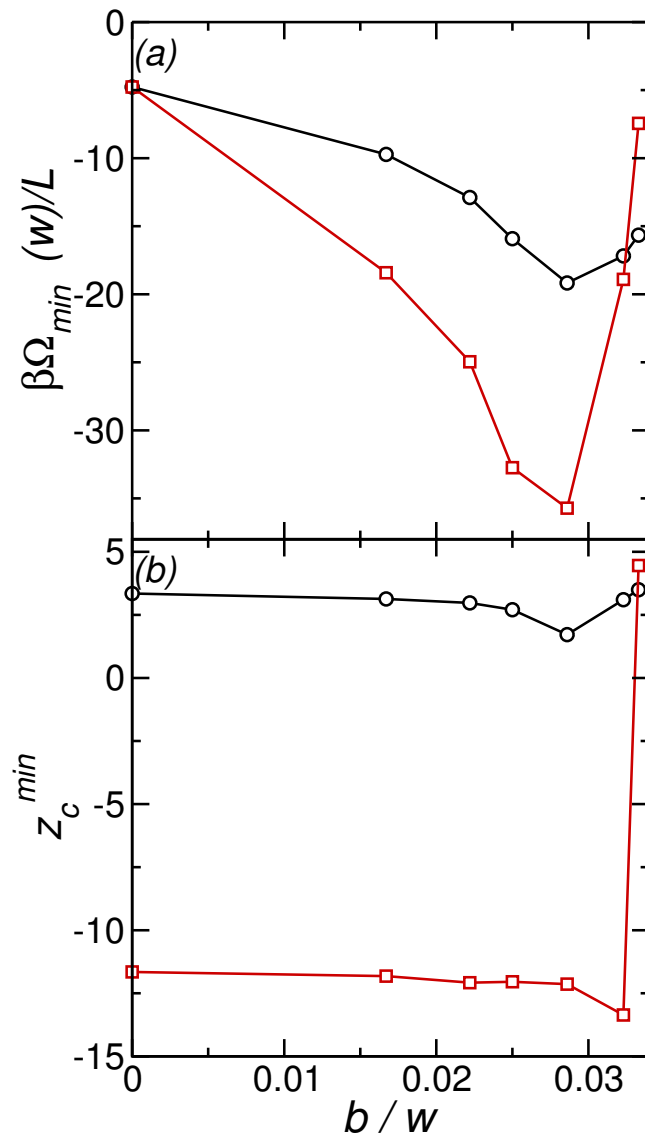


Fig. 6 D. L. Cheung and M. P. Allen

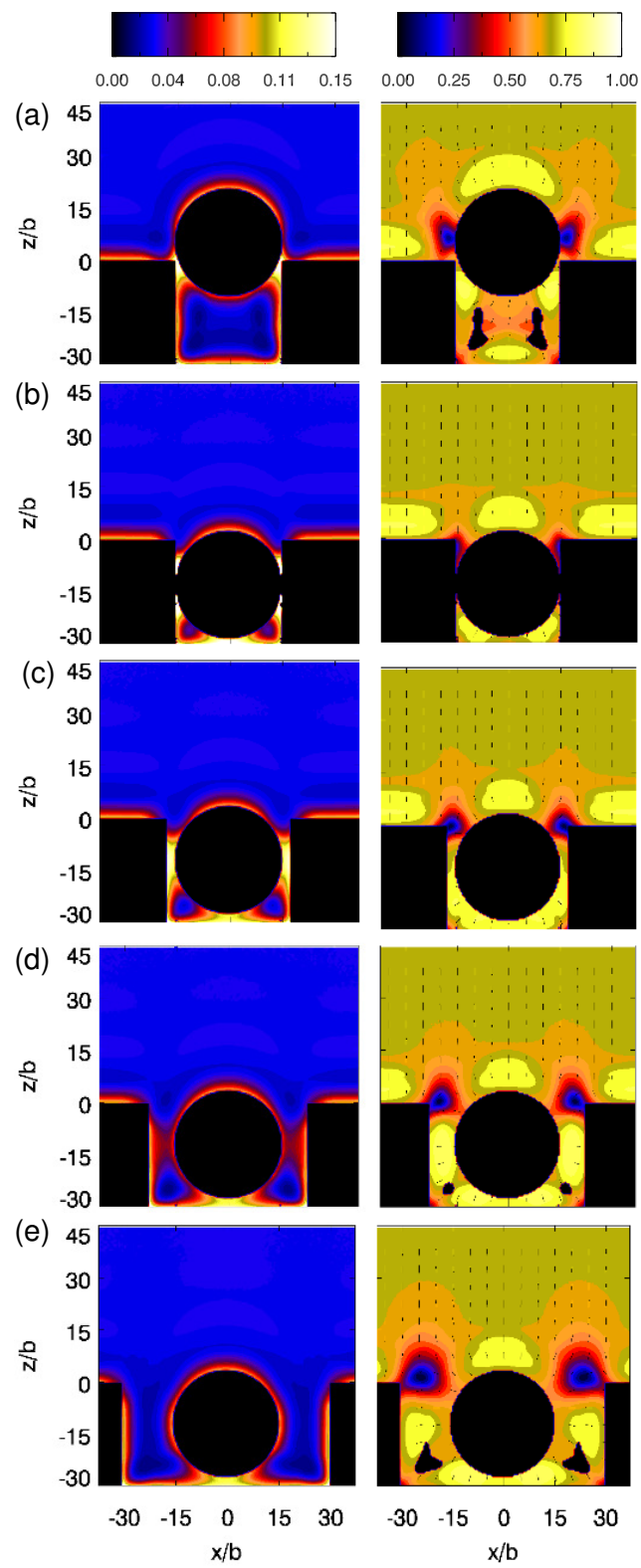


Fig. 7 D. L. Cheung and M. P. Allen

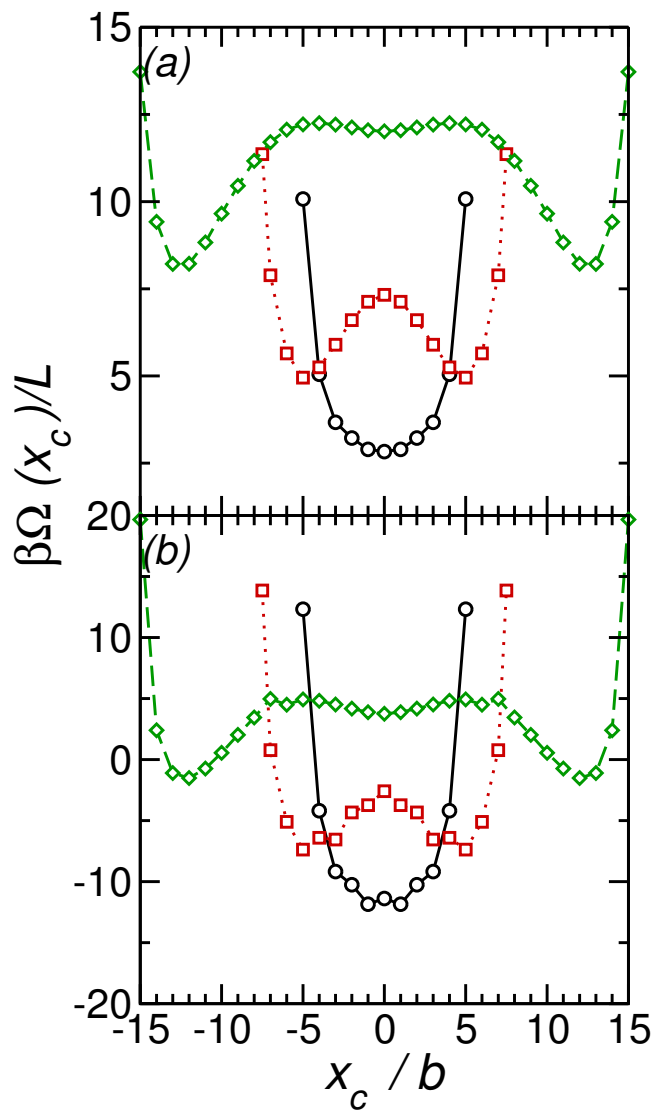


Fig. 8 D. L. Cheung and M. P. Allen

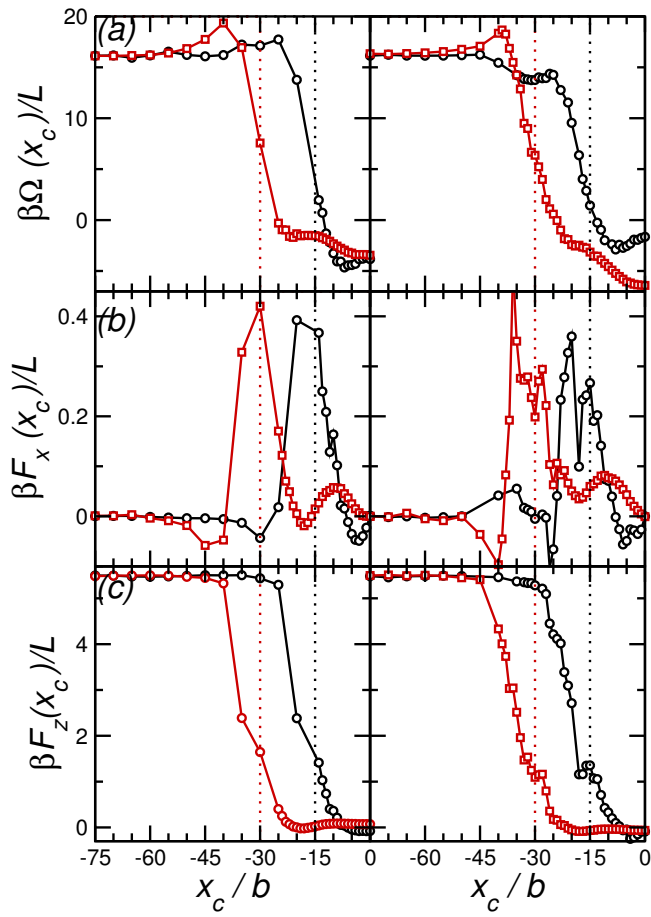


Fig. 9 D. L. Cheung and M. P. Allen

